

A Triboelectric Nanogenerator as a Self-Powered Sensor for a Soft–Rigid Hybrid Actuator

Jian Chen, Baodong Chen, Kai Han, Wei Tang,* and Zhong Lin Wang*

Triboelectric nanogenerators are a promising technology for use in self-powered sensors, which take advantage of multiple choices of materials and high response to low-frequency triggering. Here, a conductive sponge/porous silicone-based triboelectric nanogenerator (SS-TENG) is demonstrated as a tactile sensor for a hybrid actuator. To fabricate the SS-TENGs, liquid silicone and ethanol are mixed well and then infiltrated inside a conductive sponge. When heated, the ethanol evaporates from the silicone, leaving plenty of empty pores. Every pore supplies the contact and separation space for the conductive sponge and silicone to form a micro TENG, and the whole bulk makes up the SS-TENG. When deformed, the SS-TENG outputs electric signals. The open-circuit voltage linearly increases from 3.9 to 17 V as the force increases from 2.9 to 9.9 N. In addition, when touched, the electric signals generated by SS-TENGs can differentiate the corresponding objects. Finally, the SS-TENGs are integrated with a soft–rigid hybrid actuator to form a bionic skeleton–muscle–skin hybrid gripper. The gripper can catch different objects and feedback electric signals, which show great potential for use in bionic robots.

1. Introduction

Recently, the pneumatic soft actuator (PSA) has attracted many attentions. The PSA is made of silicone rubber by molding method, which takes advantages of light weight, simple fabrication, low cost, and high compliance.^[1–5] It has numerous valuable applications especially in unexpected situations and unstructured environments, such as wearable devices and service robots.^[6,7] However, the PSA also faces many challenges.^[8,9] Since the

silicone is too inert to bond with other materials, the constructed PSA is also hard to be integrated with other components for a high performance robot. In addition, the fabrication process of the PSA is based on molding and demolding, which restricts it to be made into complex structures.^[10–12] Furthermore, the PSA needs a lot of sensors to perceive its deformation and to interact with environments, due to its multidegree of freedom.^[13–18] Triboelectric nanogenerators (TENGs) can act as a self-powered sensors for the defect tolerant sensor network.^[19–23] With the advantages of wide choices of materials, flexible, light weight, high response to the low frequency triggering, the TENGs have been demonstrated as tactile and proximity sensors for human–machine interaction, which is very suitable to be applied in the PSA.^[24–30]


Here, we develop the sponge/silicone composite (SSC) as connecting material to bond a PSA with the skeleton into a soft–rigid hybrid actuator, which combines the advantages of both the traditional rigid actuator and the emerging PSA. In addition, a conductive sponge/porous silicone based triboelectric nanogenerators (SS-TENGs) are constructed as a self-powered tactile sensor. The open-circuit voltage of the SS-TENGs increases linearly from 3.9 to 17 V as the force increases from 2.9 to 9.9 N. Finally, the hybrid actuators and the SS-TENGs are integrated into a skeleton–muscle–skin hybrid actuator, and then two actuators are assembled into a gripper. The gripper can catch different objects and feedback voltage signals.

2. Results and Discussion

To evaluate the bonding ability of the SSC, different materials are bonded with SSC, and then are conducted to the peel tests. The rigid materials are fixed on the substrate by adhesive tape. The silicone is clamped to a linear motor (Linmot E1100) and stretched at a speed of 0.2 mm s⁻¹. The force is recorded by a force gauge (Handpi HP-10). As shown in **Figure 1a**, the peel strengths between silicone and structural materials are tested, which are usually used to make up the skeletons, such as Cu, Al, and acrylic. The maximum peel strengths of Cu, Al, and acrylic are 0.45, 0.40, and 0.37 N mm⁻¹ respectively. Since PCB (like epoxy-glass FR4 and Kapton) based electronic device is inevitable in soft robot. The peel strength between the silicone and PCB

J. Chen, Prof. B. D. Chen, K. Han, Prof. W. Tang, Prof. Z. L. Wang
CAS Center for Excellence in Nanoscience
Beijing Key Laboratory of Micro-nanoEnergy and Sensor
Beijing Institute of Nanoenergy and Nanosystems
Chinese Academy of Sciences
Beijing 100083, P. R. China
E-mail: tangwei@binn.cas.cn; zlwang@gatech.edu

J. Chen, Prof. B. D. Chen, K. Han, Prof. W. Tang, Prof. Z. L. Wang
School of Nanoscience and Technology
University of Chinese Academy of Sciences
Beijing 100049, P. R. China
Prof. Z. L. Wang
School of Materials Science and Engineering
Georgia Institute of Technology
Atlanta, GA 30332-0245, USA

 The ORCID identification number(s) for the author(s) of this article can be found under <https://doi.org/10.1002/admt.201900337>.

DOI: 10.1002/admt.201900337

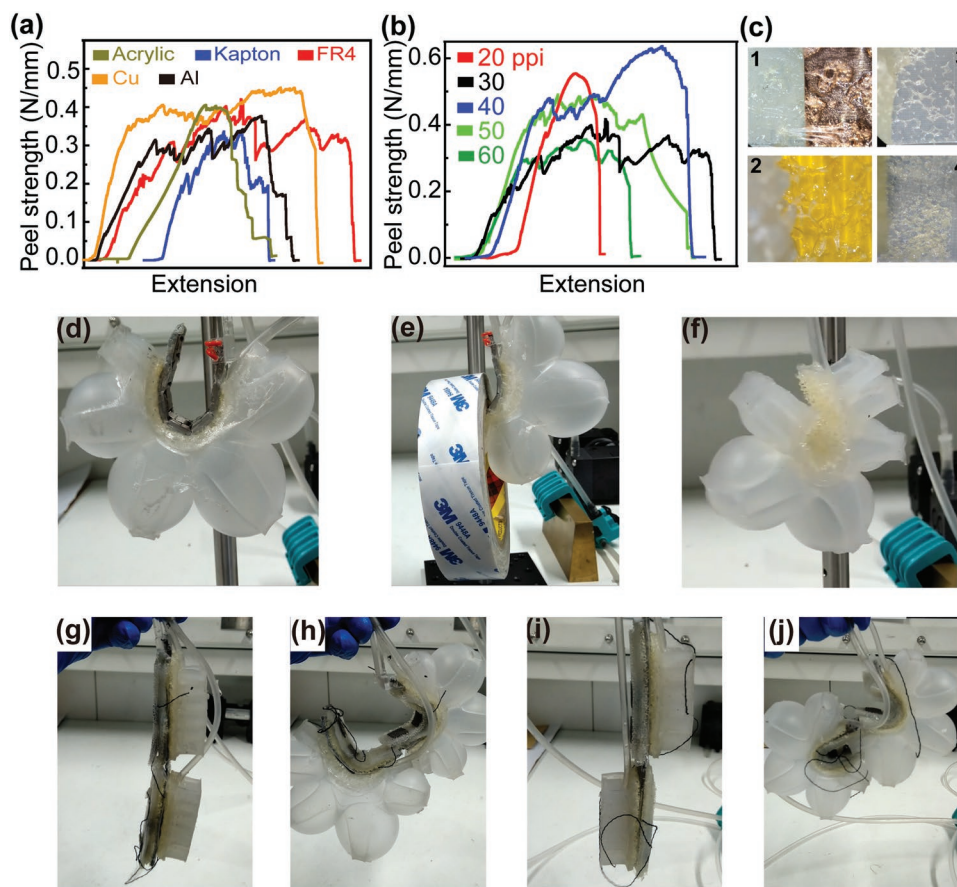


Figure 1. Investigation of the soft–rigid bonding strength and the performance of the soft–rigid hybrid actuator. a,b) The peel strength of the silicone that is bonded with different materials. c) The photograph of the break-up surface. d) The photograph of the soft–rigid hybrid actuator at pressurized state. e) The photograph of the soft–rigid hybrid actuator caught a tape. f) The photograph of a PSA at pressurized state. g) The photograph of the two soft–rigid hybrid actuators that are integrated in series, and h) curve at a “*ω*” shape when pressurized. i) The photograph of the two soft–rigid hybrid actuators are integrated in series but reversed, and j) curve at an “*S*” shape when pressurized.

substrates are also tested. The peel strengths of epoxy glass and Kapton are 0.41 and 0.3 N mm⁻¹ respectively (Figure 1a). The bonding strength of the silicone and Kapton by SSC is stronger than that by surface treatment and chemical reaction.^[31,32] The sponge is the key factor that influences the peel strength and failure mode. Five kinds of sponges with different pore densities (20, 30, 40, 50, and 60 ppi) are used to fabricate the SSCs. Then the SSCs are glued to epoxy glass. The bonding strength between different SSCs with epoxy glass are investigated. As shown in Figure 1b, the SSC with 40 ppi sponge has a better performance and the peel strength reaches up to 0.61 N mm⁻¹. The high-density sponges (50 and 60 ppi) have very fine backbone. Therefore, they are very easy to be broken up when they are made into SSC and bonded to other materials. The low-density (20 and 30 ppi) sponges are difficult to be glued with other rigid materials due to sparse backbones. The broken up surfaces are examined under microscope to investigate the failure modes. As shown in photograph 1 and 2 of Figure 1c, Cu and Kapton surfaces have some SSC residue that teared from the bulk materials, indicating the cohesive failure of the SSC. There are also some places where the sponge glue adhesive failure happens. If low-density sponges are used in the SSC, the broken-up surfaces have a little

sponge residue. This means the adhesive failure has happened due to the sponge glue (pictures 3 in Figure 1c). Meanwhile, if high-density sponges are used, cohesive failure has happened because there are many SSC residues (pictures 4 in Figure 1c). These experiments prove that the SSC is a great feasible material to bond silicone-based PSA with skeleton materials.

A soft–rigid hybrid actuator is fabricated according to the processes in Figure 2. The skeleton of the soft–rigid hybrid actuator can be well fixed at the supports by the means of traditional “nuts-and-bolts,” as shown in Figure 1d–f. Powered by air pressure, the PSA expands and drives the skeleton to bend. The deformation of the hybrid actuator starts from the fixed point, which acts as a reference for modeling and controlling the deformation of the actuator. As a comparison, the fully soft actuator (Figure 1f) has no rigid part for fixing but can just be hanged by the flexible tubing. When bended under pressure, every part of the body changes its position and configuration, which is too complex to model and control. The skeleton has also enhanced the capability of catching. As shown in Figure 1e, the hybrid actuator bends at a “*U*” shape under pressure, and can easily hook a tape. But the fully soft actuator turns at an “*r*” shape and fails to hook the tape. The comparisons are shown in Video S1 in the Supporting Information.

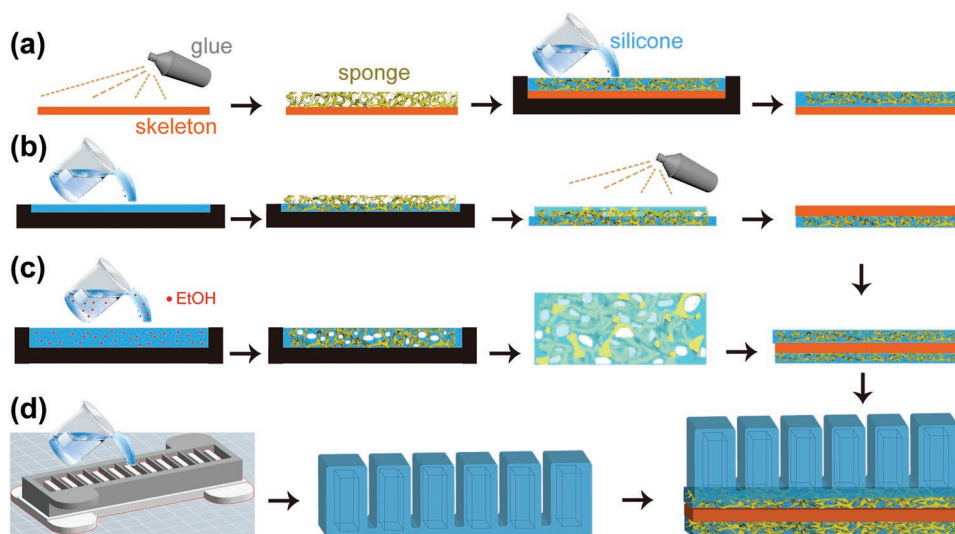


Figure 2. The fabrication processes of the hybrid actuator. a) The scheme that achieves the soft–rigid hybrid structure through the SSC. b) Another scheme that achieves the soft–rigid hybrid through the SSC. c) Fabrication process of the SS-TENGs. d) Fabrication of the PSA. Then, all the components are integrated together.

Another advantage of the hybrid actuators is that they are very easily assembled into complex structures. As shown in Figure 1g–f, two hybrid actuators are connected end-to-end in the same orientation through a hinge joint. Powered by air pressure, the two actuators bend simultaneously to form a “ ω ” shape. As shown in Figure 1i,j, when connected end-to-end but in the opposite orientation, they will bend to an “S” shape under pressure (as shown in Video S2 in the Supporting Information). Multiple hybrid actuators can be integrated to form a complex structure and work cooperatively. Therefore, the soft–rigid hybrid actuator has the virtues of more stable and better gripping capability, as well as easier to be supported and assembled.

Then, the performances of the SS-TENGs are evaluated, which is fabricated as the scheme displayed in Figure 2c. Figure S1a,b in the Supporting Information shows the SEM pictures of conductive sponge, which is used as electrode and triboelectric materials. The sizes of the backbone of conductive sponge are about 50 μm and the sizes of the cells range from 200 to 400 μm . The cross-sectional SEM images of the SS-TENGs (Figure S2a,b, Supporting Information), clearly show that the pores are randomly distributed throughout the silicone. The pores are about 0.5–1 mm in diameters, which are much larger than the cells sizes of conductive sponge. Therefore, the pores will always enclose some conductive sponge backbones. The backbone inside the pores is free of silicone and separated from the silicone internal surface. In Figure S3a,b in the Supporting Information, the EDS confirms that at the surface of the exposed sponge is covered by conductive metal Ni but not Si. Every pore supplies the contact and separation space for conductive sponge and silicone to form a micro TENGs, and the whole bulk makes up the SS-TENGs. The working principle of the SS-TENGs under period pressure is shown in Figure 3a. At initial state, the silicone is separated from the conductive sponge. When pressed, the pores are squeezed. The silicone approaches and contacts with conductive sponge. Because of triboelectrification, the silicone is negatively charged, and the

sponge is positively charged. When the force is withdrawn, the pores recover back and conductive sponge is separated from the negatively charged silicone. Due to the electrostatic induction, the electric potential of sponges increases and outputs a voltage signal. Electrons will flow into the sponge from external circuit to balance the electric field, forming a current signal. When pressed again, the silicone comes close to the conductive sponge. The potential of the sponge decreases, and the electrons flow out of the sponge, forming a reversed electric signal. The force that is applied to the SS-TENGs is recorded by the force gauge and is shown in Figure 3b. The frequency of the force is 0.28 Hz and the peak value is 2.9 N. The corresponding open-circuit voltage of the SS-TENGs is shown in Figure 3c. The peak voltage of the SS-TENGs is 3.8 V and the transferred charge is 1.4 nC (Figure 3d). The influence of the applied force to the open-circuit voltage is investigated and shown in Figure 3e. When the applied force increases from 3.9 to 9.9 N, the open-circuit voltage increases from 5.5 to 17.1 V. As shown in Figure 3f, the peak voltage is directly related to the applied force and the slope of the linear fitting equation is 1.8 V N^{-1} . Therefore, the SS-TENGs can be used as a force sensor. When SS-TENGs is bended by tweezer periodically, the SS-TENGs can also output electric signals. The voltage is about 4.5 V and the transferred charge is 1.25 nC (as shown in Figure 3g,h). To test the robustness, the SS-TENGs is periodically bended by the linear motor. The diagonally resistance of the conductive sponge is recorded and displayed in Figure 3i. The initial resistance of the sponge is 2.2 k Ω . After bending for 20 min (3000 times), the resistance increases to 3.5 k Ω , which is much lower than the matching resistance of the TENGs.

Besides, the SS-TENGs also works under the single-electrode mode. The conductive sponge is the back electrode, while the silicone is the dielectric layer for electrification. Different materials, including polytetrafluoroethylene (PTFE), Cu, polyethylene terephthalate (PET), and ordinary PU sponge, are used as free-standing layers. The open-circuit voltage and

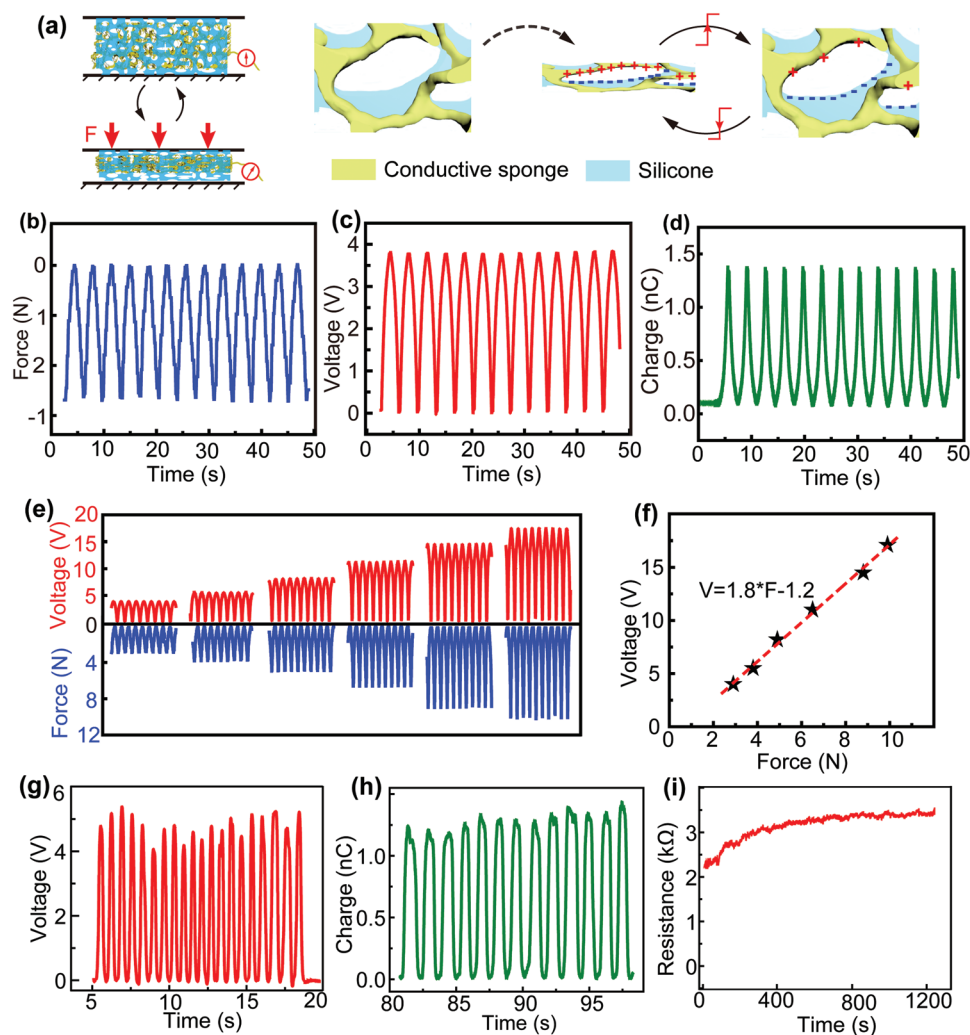


Figure 3. The working principle and output performance of SS-TENGs. a) The working principle of the SS-TENGs. b) The force that applied to the SS-TENGs. c) The open-circuit voltage, and d) the transferred charge of the SS-TENGs. e) The corresponding open-circuit voltage under different forces. f) Linear fitting of the voltages and forces. g) The open-circuit voltage and h) the transferred charge of the SS-TENGs when is bended periodically. i) The resistance of the conductive sponge during bending for 20 mins.

transferred charge are shown in **Figure 4a,b**. The voltage of PTFE is only 2.5 V, and the transferred charge is merely 1 nC. The PU sponge has the best output performance, with the voltage of 26 V and transferred charge of 8 nC. The bridged current of the PU sponge is about 0.45 μ A (Figure 4c) and a 10 μ F capacitor is charged to 1 V within 4 min (Figure 4d). In addition, the output voltages of the PU sponge are measured respectively after 1 h, 3 h, 6 h, and a month, as shown in Figure 4e. It shows no significant change, indicating a good reliability and durability.

Finally, the SS-TENGs are integrated with soft-rigid hybrid actuators to act as self-powered touch sensors. As shown in **Figure 5a,b**, when the gripper touched by a human finger, the voltage output of the SS-TENGs reaches to 15 V. However, if a pen contact with it, the voltage output is only about 5 V. Figure 5c,d shows the hybrid gripper can catch different materials with different voltage signals output. When catching a fragile bubble, output voltage of the SS-TENGs is only 4 V.

And when catch a larger and heavier bottle, the voltage output is about 12 V. To increase the reliability, more SS-TENGs could be integrated to form an array. As demonstrated in Figure 5e–g, two SS-TENGs are arranged side-by-side in a gripper. When objects are caught and dropped, the output voltages of these two SS-TENGs are complementary to each other.

3. Conclusion

In conclusion, we have developed a kind of skeleton–muscle–skin hybrid actuator. The soft-rigid hybrid architecture is achieved by the SSC material, with the bonding strength of ≈ 0.4 N mm^{-1} . The silicone-based PSA is bonded to metal skeleton, which is used for supporting and integration. An SS-TENG is fabricated and serves as a self-powered sensor. The output voltage of the SS-TENGs is linearly related to the force.

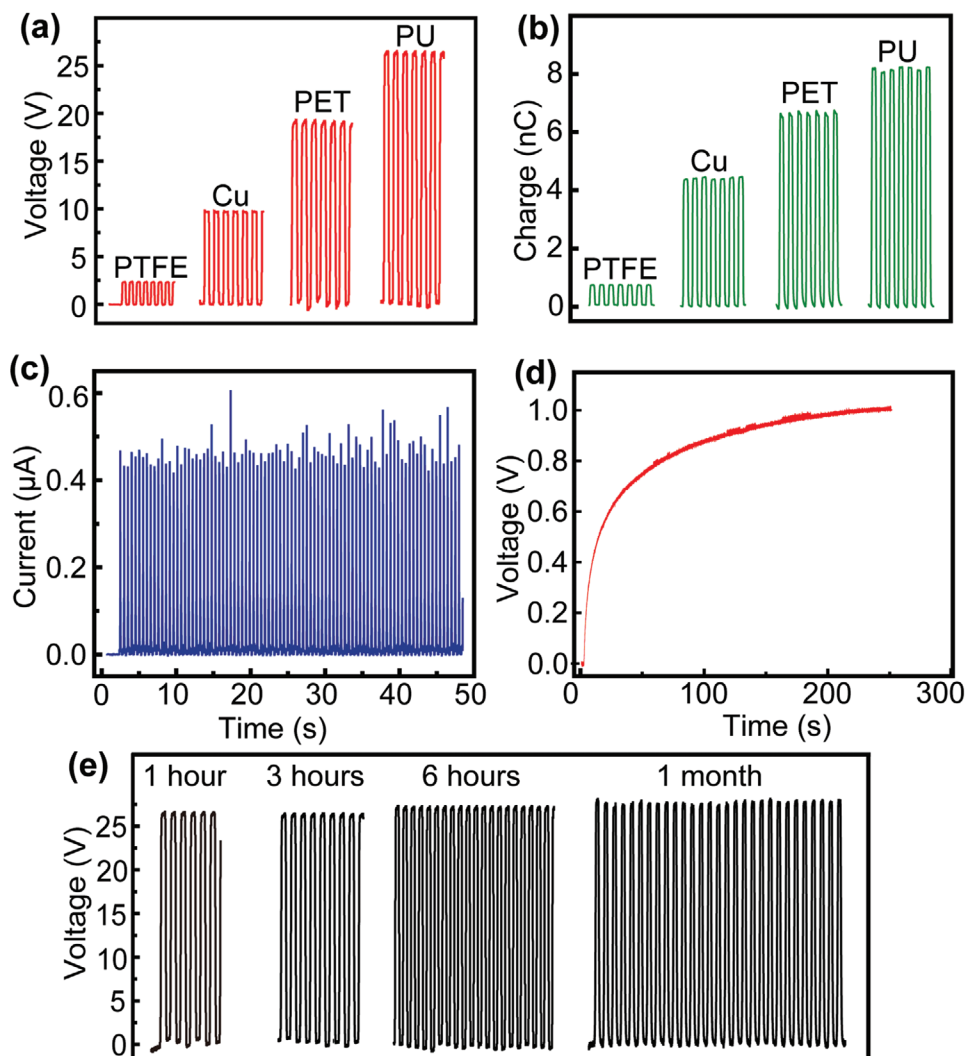


Figure 4. The output performance of the SS-TENGs when is contacted/separated with different materials. a) Open-circuit voltages and the b) the transferred charge when is contacted/separated with PTFE, Cu, PET, PU. c) The bridged short-circuit current of the SS-TENGs when is contacted/separated with PU. d) The voltage of capacitor that is charged by SS-TENGs. e) Stability and robustness testing.

And the SS-TENGs can actively respond to different materials' touch. As a demonstration, two hybrid actuators are assembled into a gripper, which could grip different objects and output voltage feedback.

4. Experimental Section

Figure 6a compares rigid gripper, soft actuator, and human finger from four aspects. The rigid gripper has high precision and large force exertion, while the soft actuator has very high structural compliance and multidegree of freedom. However, the human finger has the best comprehensive properties, which are attributed to its complex structure. The finger has rigid skeleton, flesh, muscle, skin and sensors, and they are bonded together well by the connecting tissue.

By imitating the finger's structure, a bionic skeleton-flesh-skin hybrid actuator was developed, as shown in Figure 6b. The hybrid actuator was composed of the PSA, SSC (Figure 6c), metal hinge, and SS-TENGs (Figure 6d). The PSA provided driving force just like

a muscle. The metal hinge acted as skeleton for supporting and integration. The PSA and skeleton were bonded together by the SSC. The backbone of PU sponge was embedded inside the silicone and nested within each other. At the lower surface, a thin layer of sponge was exposed outside, where could be bonded to other rigid materials by commercially available sponge glue. The upper surface of the SSC was silicone only, where could be bonded to other silicone-based components with uncured silicone. The function of the SSC was similar to the connecting tissue of creatures. The photograph of SS-TENGs is shown in Figure 6d. The conductive sponge (black color) was in the size of $16 \times 16 \times 5 \text{ mm}^3$. Finally, the SS-TENGs was bonded to the skeleton by the same method to form the bionic skeleton-flesh-skin hybrid actuator. Under pressure, the inflation of air channels caused the bending action. And then the SS-TENG output electric signals, as shown in Figure 6e.

Figure 2a shows the fabrication process of the SSC. The PU sponge (ordinary and conductive) was purchased at local stores and the ecoflex 00-30 silicone was purchased from Smooth-On, Inc. The mixed liquid silicone was poured into the 2 mm deep mold. Then, the 3 mm thick and 30 ppi (pores per inch) sponge was submerged into the uncured silicone, and the cells of the sponge were filled with silicone. Because

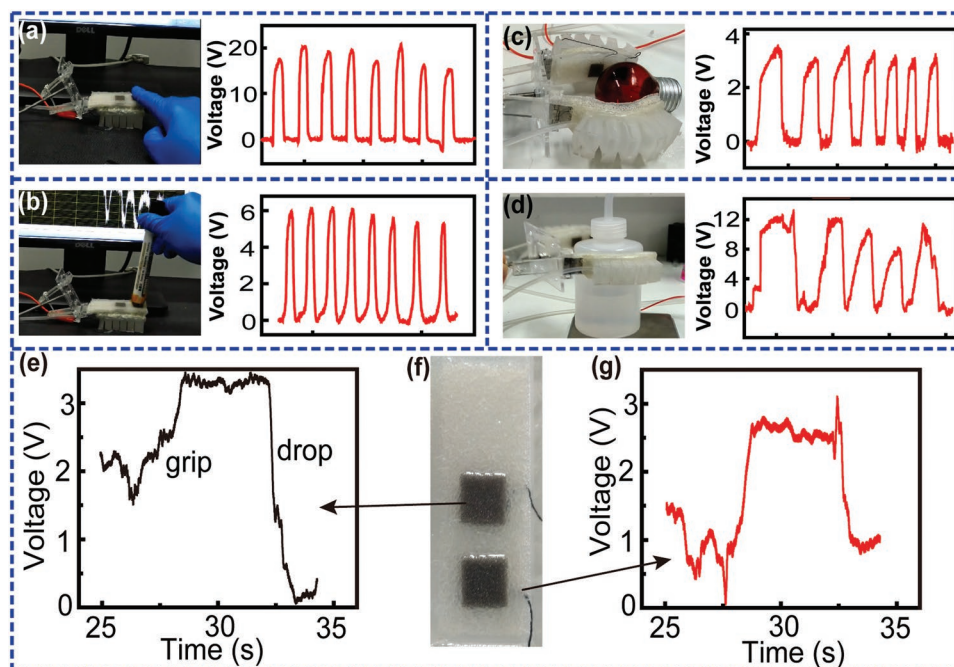


Figure 5. The performance of the hybrid gripper. a) The voltage output when the hybrid gripper is touched with a finger and b) when touched with a pen. c) The voltage output when the gripper grips a bulb and d) a bottle. e) The voltage of the first SS-TENGs and g) the voltage of the second SS-TENGs when the hybrid gripper catches a plastic cup and drops it. f) The photograph of the SS-TENGs array.

of the sponge's 3D porous backbone networks, the sponge and silicone were tightly nested within each other after being cured under 80 °C for 0.5 h, and formed an SSC. At the upper surface, a thin layer of bare sponge was exposed outside because it was thicker than the silicone. The other materials (like metals, plastics, leathers, and woods) could be firmly adhered to that layer of sponge by glue. The lower surface of the SSC was a layer of silicone, where could be adhered to other silicone-based components by uncured silicone. In this way, the silicone can be adhered to other rigid materials to achieve the soft-rigid hybrid structure. Figure 2b depicts another fabrication process. The sponge was glued to the rigid materials by sponge glue first. Then, the liquid silicone was soaked and infiltrated into the sponge. After being cured, the soft silicone was stuck with the rigid materials through the sponge.

Figure 2c shows the fabrication process of SS-TENGs. The liquid silicone and 10 wt% ethanol were mixed well and then poured into the

5 mm deep mold. Then, the conductive sponge was cut into the same size of the mold and immersed into the mixture. The sponge would soak up the mixture. When heated at 60 °C, the ethanol evaporated and expanded to form small bubbles throughout the silicone during the curing. Then, heated at 85 °C for 2 h, the ethanol boiled (boiling point at 78.3 °C)^[5,33] evaporated, and leaked out from the silicone, leaving the empty pores. The conductive sponge, pores, and silicone substrate made up the SS-TENGs. As shown in Figure 2d, the PSA was fabricated by molding process. The liquid silicone was poured into the 3D-printed mold and fully cured at 80 °C for 0.5 h to form the channel part. The channel part was sealed by bonding to the silicone side of the SSC. And the sponge side of the SSC was bonded to the metal hinge skeleton. The SS-TENGs was adhered to the skeleton in the same way and served as a self-powered sensor. Finally, the soft actuator, hinge skeleton and SS-TENGs were assembled together as a bionic skeleton–muscle–skin hybrid actuator.

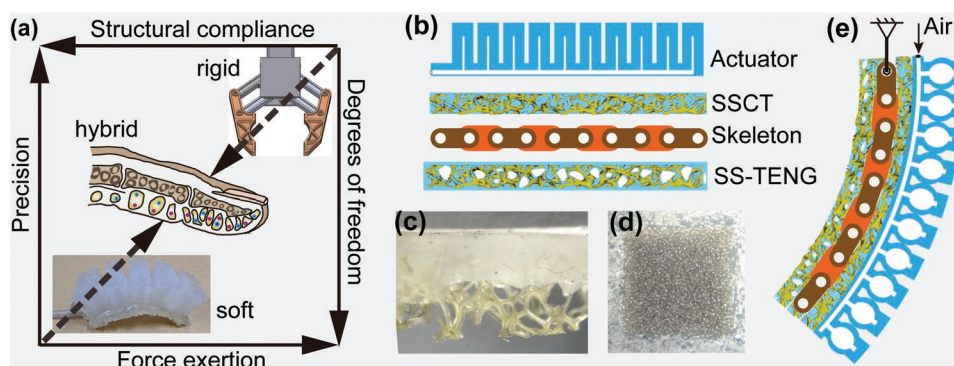


Figure 6. Illustration of the soft-rigid hybrid actuator. a) The comparison of the properties between soft actuator, rigid gripper, and human finger. b) The major components of the soft-rigid hybrid actuator. c) The photograph of the SSC material. d) The photograph of SS-TENGs. e) Schematic diagram of the skeleton–muscle–skin hybrid actuator after being assembled.

Supporting Information

Supporting Information is available from the Wiley Online Library or from the author.

Acknowledgements

J.C. and B.D.C. contributed equally to this work. Research was sponsored by the National Key R & D Project from Minister of Science and Technology (2016YFA0202704), the National Science Foundation of China (DMR-1505319) (materials synthesis and application in sensors), Beijing Municipal Science & Technology Commission (Z171100000317001, Z171100002017017, and Y3993113DF), and National Natural Science Foundation of China (Grant Nos. 51432005, 5151101243, and 51561145021).

Conflict of Interest

The authors declare no conflict of interest.

Keywords

hybrid actuator, self-powered sensors, sponge, triboelectric nanogenerator

Received: April 23, 2019

Revised: June 3, 2019

Published online:

- [1] D. Rus, M. T. Tolley, *Nature* **2015**, 521, 467.
- [2] G.-Z. Yang, R. J. Full, N. Jacobstein, P. Fischer, J. Bellingham, H. Choset, H. Christensen, P. Dario, B. J. Nelson, R. Taylor, *Sci. Rob.* **2019**, 4, eaaw1826.
- [3] M. A. Robertson, J. Paik, *Sci. Rob.* **2017**, 2, eaan6357.
- [4] P. Boyraz, G. Runge, A. Raatz, *Actuators* **2018**, 7, 48.
- [5] A. Miriyev, K. Stack, H. Lipson, *Nat. Commun.* **2017**, 8, 596.
- [6] L. Cappello, K. C. Galloway, S. Sanan, D. A. Wagner, R. Granberry, S. Engelhardt, F. L. Haufe, J. D. Peisner, C. J. Walsh, *Soft Rob.* **2018**, 5, 662.
- [7] P. Polygerinos, N. Correll, S. A. Morin, B. Mosadegh, C. D. Onal, K. Petersen, M. Cianchetti, M. T. Tolley, R. F. Shepherd, *Adv. Eng. Mater.* **2017**, 19, 1700016.
- [8] G. Yang, J. Bellingham, P. E. Dupont, P. Fischer, L. Floridi, R. Full, N. Jacobstein, V. Kumar, M. McNutt, R. Merrifield, B. J. Nelson, B. Scassellati, M. Taddeo, R. Taylor, M. Veloso, Z. L. Wang, R. Wood, *Sci. Rob.* **2018**, 3, eaar7650.
- [9] H. Lipson, *Soft Rob.* **2014**, 1, 21.
- [10] S. Yoshida, Y. Morimoto, L. Zheng, H. Onoe, S. Takeuchi, *Soft Rob.* **2018**, 5, 718.
- [11] Y. Chen, F. Wan, T. Wu, C. Song, *J. Micromech. Microeng.* **2018**, 28, 014007.
- [12] Y. Jiang, D. Chen, C. Liu, J. Li, *Soft Rob.* **2019**, 6, 118.
- [13] T. G. Thuruthel, B. Shih, C. Laschi, M. T. Tolley, *Sci. Rob.* **2019**, 4, eaav1488.
- [14] H. A. Sonar, J. Paik, *Front. Rob. AI* **2016**, 2, 1.
- [15] C. M. Boutry, M. Negre, M. Jorda, O. Vardoulis, A. Chortos, O. Khatib, Z. Bao, *Sci. Rob.* **2018**, 3, eaau6914.
- [16] D. Yamamoto, S. Nakata, K. Kanao, T. Arie, S. Akita, K. Takei, *Adv. Mater. Technol.* **2017**, 2, 1700057.
- [17] T. Yamaguchi, T. Kashiwagi, T. Arie, S. Akita, K. Takei, *Adv. Intell. Syst.* **2019**, <https://doi.org/10.1002/aisy.201900018>.
- [18] K. Xu, Y. Lu, K. Takei, *Adv. Mater. Technol.* **2019**, 4, 1800628.
- [19] Y.-C. Lai, J. Deng, R. Liu, Y.-C. Hsiao, S. L. Zhang, W. Peng, H.-M. Wu, X. Wang, Z. L. Wang, *Adv. Mater.* **2018**, 30, 1801114.
- [20] Q. Hua, J. Sun, H. Liu, R. Bao, R. Yu, J. Zhai, C. Pan, Z. L. Wang, *Nat. Commun.* **2018**, 9, 244.
- [21] X. Wang, Y. Yin, F. Yi, K. Dai, S. Niu, Y. Han, Y. Zhang, Z. You, *Nano Energy* **2017**, 39, 429.
- [22] H. Guo, X. Pu, J. Chen, Y. Meng, M.-H. Yeh, G. Liu, Q. Tang, B. Chen, D. Liu, S. Qi, C. Wu, C. Hu, J. Wang, Z. L. Wang, *Sci. Rob.* **2018**, 3, eaat2516.
- [23] Z. L. Wang, *Nano Energy* **2019**, 58, 669.
- [24] T. Li, Y. Xu, M. Willander, F. Xing, X. Cao, N. Wang, Z. L. Wang, *Adv. Funct. Mater.* **2016**, 26, 4370.
- [25] H. Zou, Y. Zhang, L. Guo, P. Wang, X. He, G. Dai, H. Zheng, C. Chen, A. C. Wang, C. Xu, Z. L. Wang, *Nat. Commun.* **2019**, 10, 1427.
- [26] A. C. Wang, C. Wu, D. Pisignano, Z. L. Wang, L. Persano, *J. Appl. Polym. Sci.* **2018**, 135, 45674.
- [27] H. Chen, Y. Song, X. Cheng, H. Zhang, *Nano Energy* **2019**, 56, 252.
- [28] X. Pu, H. Guo, Q. Tang, J. Chen, L. Feng, G. Liu, X. Wang, Y. Xi, C. Hu, Z. L. Wang, *Nano Energy* **2018**, 54, 453.
- [29] T. Liu, M. Liu, S. Dou, J. Sun, Z. Cong, C. Jiang, C. Du, X. Pu, W. Hu, Z. L. Wang, *ACS Nano* **2018**, 12, 2818.
- [30] Z. L. Wang, J. Chen, L. Lin, *Energy Environ. Sci.* **2015**, 8, 2250.
- [31] M. V Hoang, H. J. Chung, A. L. Elias, *J. Micromech. Microeng.* **2016**, 26, 105019.
- [32] Q. Liu, G. Nian, C. Yang, S. Qu, Z. Suo, *Nat. Commun.* **2018**, 9, 846.
- [33] A. Miriyev, G. Caires, H. Lipson, *Mater. Des.* **2018**, 145, 232.